CHEMPHYSCHEM

DOI: 10.1002/cphc.200800829

Self-Propelled Polymer Nanomotors

Yu-Guo Tao* and Raymond Kapral*[a]

Molecular motors that use chemical reactions to drive directed motion are widespread in nature.[1] In addition to biochemical motors,[2] which play an important role in the biochemistry of the cell, a wide variety of synthetic molecular motors that make use of chemical energy, light, magnetic fields and other sources of energy to effect motion have been constructed. These include molecular motors that rely on asymmetrical conformational changes, similar to many biological motors or self-propelled bacteria, as well as motors that make use of chemical catalysis and an asymmetrical distribution of reaction products to effect motion.[3–12] The basic elements that are important for the operation and directed motion of these nonequilibrium nanodevices are an intrinsic asymmetry and a power source that maintains the system out of equilibrium. Models for motors that operate by conformational changes and asymmetric gradients have been constructed and used to elucidate the nature of the propulsion mechanisms.[13–15] Self-propelled nanodimers, which consist of linked catalytic and noncatalytic spheres, are simple examples of such molecular motors.[16,17] A chemical reaction $A \rightarrow B$ occurs on the catalytic sphere. The asymmetric spatial distribution of the B molecules produced in the reaction gives rise to a directed force on the dimer that propels it in solution. This is a nonequilibrium nanodevice that consumes fuel in its environment, uses it to generate a nonequilibrium local spatial distribution of products, which in turn gives rise to directed motion.

Herein, we show how polymer molecules can be modified to function as molecular motors. By attaching a nanocolloidal particle or molecular group that catalyzes a chemical reaction to the end of a polymer chain, the diffusive motion of the polymer in solution can be converted into directed motion provided certain design conditions are satisfied. The polymer molecules respond to self-generated chemical concentration gradients by moving in specific directions determined by the forces on the polymer chain. We describe the mechanism that is responsible for such motion, discuss the factors that must be taken into account when designing polymers with specific directional motion characteristics, and illustrate our results with particle-based simulations of self-propelled polymer dynamics in solution. Polymer molecules that are able to move in a directed fashion, instead of simply executing a diffusive random walk to explore configuration space, are able to perform certain tasks more effectively. For example, since the polymers respond to self-generated gradients, they can be designed to seek each other in solution, thus aiding polymerization, self-assembly or targeted chemical reaction dynamics.

Simulations play a central role in the investigation of the factors leading to the self-propelled motion of polymer nanomotors and herein we provide some details of how the polymer motors are constructed and their dynamics is studied. The solvent comprises a large number of point-like A and B molecules. We consider a bead-spring model of a polymer to the end of which we attach a nanocatalytic particle C with diameter d_C.[18] An irreversible chemical reaction, $A + C \rightarrow B + C$, occurs at the catalytic sphere with probability p_R whenever A encounters C.[19] Both A and B molecules interact with the C sphere through repulsive Lennard-Jones (LJ) potentials with energy parameter ε_C and distance parameter σ_C. Repulsive LJ forces act between A solvent molecules, which constitute the majority of molecules in the solution, and the polymer beads. The B molecules interact with the polymer beads through truncated attractive LJ potentials. The interactions between neighbouring polymer beads are governed by finite extensible nonlinear elastic (FENE) potentials[20] while repulsive or attractive LJ forces act among all polymer beads. The former case models good solvent conditions where the polymer chain is in an extended configuration; the later case models a poor solvent where the polymer chain is in a collapsed globular state.

In addition to the polymer chain, the system contains a large number of solution molecules. The most effective way to incorporate the solvent is through mesoscopic models that are able to bridge the large length and timescale gaps that characterize the solvent and polymer dynamics. A variety of such methods have been proposed including the lattice Boltzmann (LB) method,[21] dissipative particle dynamics (DPD)[22] and multiparticle collision (MPC) dynamics.[23–26] The LB method is designed to simulate the Boltzmann equation on a grid and uses simplified collision rules that locally conserve mass and momentum to guarantee the correct Navier–Stokes hydrodynamics. DPD is an off-lattice hydrodynamic method, in which soft-repulsive interaction potentials and the pair-wise Langevin thermostat are applied. In DPD several atoms are grouped into simulation sites whose dynamics is governed by conservative and frictional forces designed to reproduce the thermodynamics and hydrodynamics of the system. The DPD particle does not describe a solvent molecule but a fluid element, which represents clusters of solvent molecules.

Herein, the solvent dynamics is modelled at a mesoscopic particle-based level using MPC dynamics. In MPC dynamics, fictitious solvent particles, representing coarse-grained real molecules, free stream and undergo effective collisions at discrete

---

[a] Dr. Y.-G. Tao, Prof. R. Kapral
Chemical Physics Theory Group
Department of Chemistry, University of Toronto
Toronto, Ontario M5S 3H6 (Canada)
Fax: (416)-978-5325
E-mail: ytao@chem.utoronto.ca
rkapral@chem.utoronto.ca

Supporting information for this article is available on the WWW under http://dx.doi.org/10.1002/cphc.200800829.

time intervals τ, which account for the effects of many real collisions during this time interval. To carry out collisions, the system is divided into a grid of cells ξ. Rotation operators $\hat{\omega}_\xi$, chosen from a set, are assigned to each cell of the system at the time of collision. Particles within each cell collide with each other and the postcollision velocity of particle i in a cell ξ is given by $\mathbf{v}'_i = \mathbf{V}_\xi + \hat{\omega}_\xi(\mathbf{v}_i - \mathbf{V}_\xi)$, where $\mathbf{V}_\xi$ is the center-of-mass velocity of particles in cell ξ. In order to insure that Galilean invariance is satisfied, a random shift of the lattice is carried out before the collision step. This mesoscopic dynamics preserves the essential features of full molecular dynamics. In particular, it conserves mass, momentum and energy so that hydrodynamic interactions, crucial for a correct description of the polymer dynamics, are automatically incorporated in the description.

The self-propelled polymer is dissolved in a solvent of A and B molecules in a cubic box (with periodic boundary conditions) of volume V.[27] In order to maintain the system in a nonequilibrium steady state where directed motion does not cease due to consumption of A in the irreversible chemical reaction, B molecules are converted back to A when they diffuse far enough away from the polymer. This mimics the input of A and removal of B by matter fluxes into and out of the system to produce a far-from-equilibrium steady state.

Figure 1 shows an instantaneous configuration of B molecules in the vicinity of the polymer motor in the steady state regime. The inhomogeneous nonequilibrium nature of the B particle density field is evident. With repulsive interactions among the polymer beads, the polymer chain exists in an extended state, while it collapses to a globular form when attractive forces operate. The chain dynamics was analyzed by computing the time variation of the radius of gyration $Rg(t) = \sqrt{N_\mathrm{P}^{-1}\sum_{i=1}^{N_\mathrm{P}} |\mathbf{r}_i(t) - \mathbf{r}_\mathrm{cm}(t)|^2}$, where $\mathbf{r}_i$ is the position of bead i and $\mathbf{r}_\mathrm{cm}$ is the center of mass of the polymer chain composed of N_P beads. The upper fluctuating curve in Figure 2a shows a large value of Rg as expected for an extended flexible polymer chain in a good solvent, while in a poor solvent Rg has a small magnitude and exhibits only small variations indicating a strongly collapsed polymer chain.

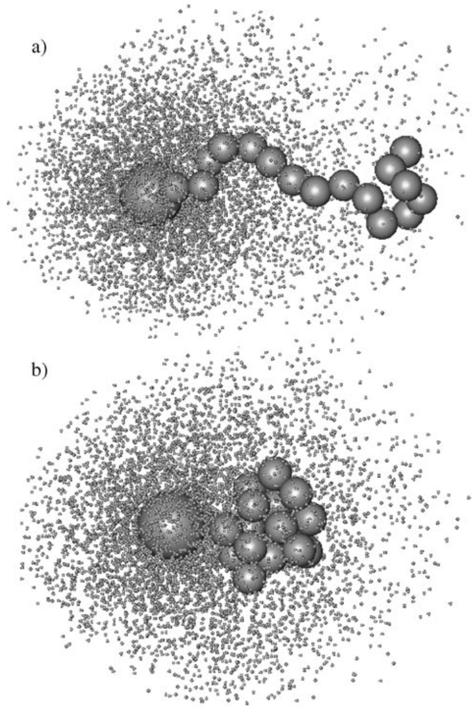

Figure 1. Instantaneous configuratins of B molecules in the vicinity of the polymer chain in a) good and b) poor solvents. The large sphere is the catalytic head of the chain while the small spheres are the noncatalytic polymer chain beads. For clarity, only the B molecules in the vicinity of the self-propelled polymer are shown in these instantaneous configurations.

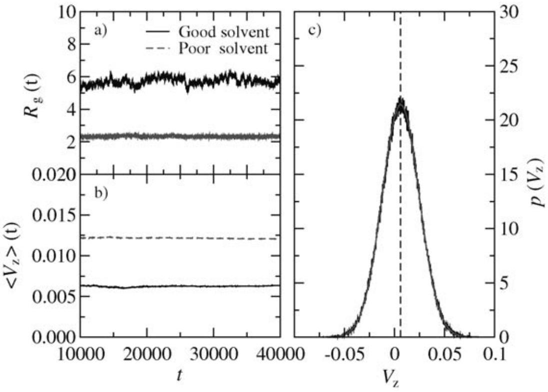

Figure 2. a) Polymer radius of gyration versus time. (The polymer consists of a catalytic head with diameter $d_\mathrm{C} = 4.0$ and 16 noncatalytic beads with $d_\mathrm{N} = 2.0$.) b) Time evolution of running averages of the polymer center-of-mass velocity along the axis between the center of the catalytic C sphere and the center-of-mass of the polymer tail. (——) and (-----) correspond to systems in which the polymer is immersed in good and poor solvents, respectively. c) Probability distribution function of V_z. (-----) is the mean velocities fit by the Maxwell–Boltzmann distribution.

The ability of the self-propelled polymer to execute directed motion is best determined by monitoring the mean value of the center of mass velocity of the polymer motor projected along the axis between the catalytic head and the center of mass of the polymer chain tail: $V_z \equiv \left\langle \mathbf{V}(t) \cdot \hat{\mathbf{z}}(t) \right\rangle$, where the angular brackets denote a time average and is the unit vector along this axis. Figure 2b shows the time evolution of $\langle V_z \rangle$ averaged over 20 realizations of the evolution. In a good solvent, $V_z \approx 0.0062$, indicating that the polymer motor moves in the direction of the catalytic head (see the video in the Supporting Information). The magnitude and nature of the directed motion is strongly influenced by the polymer chain dynamics. In good solvents, longer extended chains are more difficult to reorient than shorter chains; however, strong chain fluctuations introduce a time variation in the direction along which the propulsion force acts. This variation causes the polymer motor to reorient. The interplay between these effects is responsible for the ultimate nature of the directed motion.

In a poor solvent, where the polymer has a compact globular structure, the motor moves faster, $V_z \approx 0.0122$, under the same propulsion conditions (see Figure 2 b). The more rapid motion is due to a smaller frictional force on the compact polymer. Because of the conformational asymmetry of the collapsed polymer chain, rotational motion is more rapid than that for symmetric nanodimers.[17]

The polymer motor velocity can be computed from an analysis of the forces that act on it, in conjunction with an examination of the reactive species nonequilibrium distributions and polymer chain conformations. The average force on the fixed polymer motor center of mass along can be written as Equation (1):

$$\begin{aligned}\left\langle \hat{\mathbf{z}}\cdot\mathbf{F}\right\rangle = & -\sum_{\alpha=\mathrm{A}}^{\mathrm{B}}\int d\mathbf{r}(\hat{\mathbf{z}}\cdot\hat{\mathbf{r}})\frac{\partial V_{\alpha\mathrm{C}}(r)}{\partial r}n_{\alpha}(\mathbf{r}) \\ & -\sum_{\alpha=\mathrm{A,B}}^{\mathrm{B}}\int d\mathbf{r}d\mathbf{r}'(\hat{\mathbf{z}}\cdot\hat{\mathbf{r}}')\frac{\partial V_{\alpha\mathrm{P}}(r')}{\partial r'}n_{\alpha\mathrm{P}}(\mathbf{r},\mathbf{r}')\end{aligned} \tag{1}$$

Here $V_{\alpha\mathrm{C}}(\mathbf{r})$ is the potential energy between a solvent molecule of species $\alpha = \mathrm{A,B}$ and the catalytic sphere, and $V_{\alpha\mathrm{P}}(\mathbf{r})$ is the potential energy between a solvent molecule of species α and a polymer bead. The origins of $\mathbf{r}$ and $\mathbf{r}'$ are on the catalytic head group and polymer bead, respectively. The average density of chemical species α at point $\mathbf{r}$ in the steady state is $n_{\alpha}(\mathbf{r})$ while $n_{\alpha\mathrm{P}}(\mathbf{r},\mathbf{r}')$ is the average steady-state two-particle solvent–polymer bead density.

The polymer motor velocity in the steady state is found by equating the average frictional force on the motor, ξV_z, with the force on the fixed polymer arising from the nonequilibrium concentration distribution: $V_z \equiv \left\langle \hat{\mathbf{z}}\cdot\mathbf{V}\right\rangle = \zeta^{-1}\left\langle \hat{\mathbf{z}}\cdot\mathbf{F}\right\rangle$, where ζ is the friction coefficient of the motor. From this expression we see that self-propelled motion relies on the existence of a nonequilibrium concentration gradient across the motor, in combination with different forces acting on the polymer chain for A and B molecules. In particular, if the nonequilibrium densities in Equation (1) are replaced by equilibrium densities, the average force vanishes. Consequently, the steady-state densities are an essential ingredient in the computation of the average force on the polymer motor. The average steady-state density $n_{\alpha\mathrm{P}}(\mathbf{r},\mathbf{r}')$ depends on the configuration of the polymer chain. In Figure 3, the probability distributions of the polymer beads parallel and perpendicular to $\hat{\mathbf{z}}$ is plotted. Figure 3 a shows that the polymer bead distribution is approximately uniform along most of the extended chain; it falls to zero near the polymer head due to the bond constraint and near the polymer tail as expected. Figure 3 b shows that most of the bead density is concentrated in a narrow tube perpendicular to $\hat{\mathbf{z}}$. To estimate V_z, the polymer motor is held fixed and $\left\langle \hat{\mathbf{z}}\cdot\mathbf{F}\right\rangle$ is computed from a time average. (This force can also be computed analytically if the nonequilibrium density fields are estimated by solving the diffusion equation subject to boundary conditions appropriate for the reaction.) The friction coefficient of the motor, ζ, may be estimated from an average over configurations of the configuration-dependent friction coefficient of the polymer in the Oseen approximation,[28] which takes the hydrodynamic interactions into account. These simple calculations yield $V_z = 0.0047$, which is slightly smaller than the simulation results (0.0062). Much of this discrepancy can be attributed to the use of the Oseen approximation for the friction tensor.

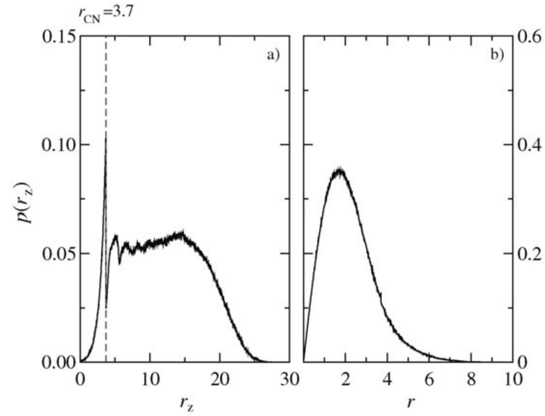

Figure 3. a) Probability distribution function of polymer beads along the vector from the catalytic head to the noncatalytic polymer center of mass, $\hat{\mathbf{z}}$. b) Probability distribution function of the flexible polymer chain perpendicular to $\hat{\mathbf{z}}$. In this example, we simulate a flexible polymer in a good solvent.

Another important element which affects the polymer motor dynamics is the chain length. Figure 4 show the influence of polymer length on the average velocity of the directed movement. We consider polymers with $N_P = 8$, 16 and 32 beads. In a good solvent, large driving forces are achieved for polymers with short chain lengths. Worm-like directed motions with relatively high velocities are observed in systems where catalytic head diameters are $d_C = 4.0$ and 8.0. The directed polymer motor motion dominates Brownian motion. In contrast, the dynamics of the 33-bead motors (catalytic head plus 32-bead tail) are strongly affected by polymer chain conformational fluctuations. As can be seen from the results for the V_z probability distribution in Figure 4 b, the mean velocity of the polymer motor is considerably smaller than its dispersion.

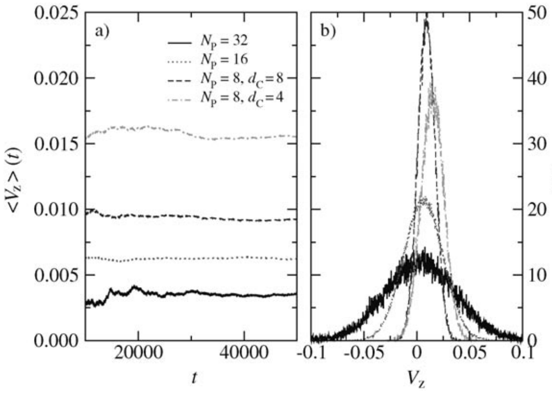

Figure 4. a) Time evolution of the running averages of the center-of-mass velocity of polymers with various numbers of noncatalytic beads along $\hat{\mathbf{z}}$. b) Probability distribution functions of V_z. The sizes of the 33-bead-polymer and the 17-bead-polymer are $d_C = 3.0$; $d_N = 1.0$ and $d_C = 4.0$; $d_N = 2.0$, respectively. Two types of 9-bead-polymers are made up of noncatalytic beads with $d_N = 4.0$ and catalytic head spheres with $d_C = 4.0$ or 8.0.

We observe that the average velocity of the polymer motor with $d_C = 4.0$ ($V_z \approx 0.016$) is about 1.7 times higher than that of a motor with $d_C = 8.0$ ($V_z \approx 0.009$) for $N_P = 8$. The change in size of the catalytic head gives rise to two competing effects on the self-propelled polymer velocity along $\hat{\mathbf{z}}$. Increasing the size of the catalytic head sphere leads to a larger chemical reaction rate which results in a higher nonequilibrium density gradient of B molecules in the vicinity of the polymer chain. However, head size increase also increases the frictional force which tends to decrease the velocity. These considerations should be taken into account when designing polymer nanomotors.

Our results have shown how self-propelled polymers can be constructed and we have identified the essential elements that enter into the design of such molecular motors. Polymer lengths, catalytic head and bead sizes, as well as interaction potentials play key roles in the design of motors whose velocities are large enough to overcome the effects of nanoscale Brownian thermal fluctuations. In particular, for rigid rod-like short-chain polymers, thermal conformational fluctuations are not strong and autonomous directed polymer motion is easily achieved. For flexible long-chain polymer motors in good solvents, directed motion must compete with strong Brownian conformational fluctuations that lead to reorientation of the self-propelled polymer. By designing polymers with different conformational dynamics and different catalytic head groups, one can construct polymer motors that either execute strong directed motion, that is, they travel long distances before they reorient, or execute Brownian diffusion, but with enhanced diffusion to explore wider regions of space. Consequently, such self-propelled polymer motors may be made to perform some tasks better than ordinary polymers. While the uses of such devices are a topic of future research, possible applications might include directed synthesis where polymer motors exploit nonequilibrium concentration gradients to find their targets, and more rapid exploration of space to increase rates of diffusion-influenced reactions.

Acknowledgement

Research supported in part by a grant from the Natural Sciences and Engineering Research Council of Canada.

Keywords: catalysis · mesoscopic dynamics · molecular motors · polymers · solvent effects

[1] See a recent review article, E. R. Kay, D. A. Leigh, F. Zerbetto, *Angew. Chem.* **2007**, *119*, 72–196; *Angew. Chem. Int. Ed.* **2007**, *46*, 72–191, and references therein.

[2] C. Mavroidis, A. Dubey, M. L. Yarmush, *Annu. Rev. Biomed. Eng.* **2004**, *6*, 363–395.

[3] R. F. Ismagilov, A. Schwartz, N. Bowden, G. M. Whitesides, *Angew. Chem.* **2002**, *114*, 674–676; *Angew. Chem. Int. Ed.* **2002**, *41*, 652–654.

[4] W. F. Paxton, K. C. Kistler, C. C. Olmeda, A. Sen, S. K. St. Angelo, Y. Cao, T. E. Mallouk, P. E. Lammert, V. H. Crespi, *J. Am. Chem. Soc.* **2004**, *126*, 13 424–13 431.

[5] S. Fournier-Bidoz, A. C. Arsenault, I. Manners, G. A. Ozin, *Chem. Commun.* **2005**, 441–443.

[6] W. F. Paxton, A. Sen, T. E. Mallouk, *Chem. Eur. J.* **2005**, *11*, 6462–6470.

[7] G. A. Ozin, I. Manners, S. Fournier-Bidoz, A. C. Arsenault, *Adv. Mater.* **2005**, *17*, 3011–3018.

[8] Y. Wang, R. M. Hernandez, D. J. Bartlett, J. M. Bingham, T. R. Kline, A. Sen, T. E. Mallouk, *Langmuir* **2006**, *22*, 10 451–10 456.

[9] H. H. Kung, M. C. Kung, *Appl. Catal. A* **2006**, *309*, 159–161.

[10] J. R. Howse, R. A. L. Jones, A. J. Ryan, T. Gough, R. Vafabakhsh, R. Golestanian, *Phys. Rev. Lett.* **2007**, *99*, 048 102.

[11] L. Qin, M. J. Banholzer, X. Xu, L. Huang, C. A. Mirkin, *J. Am. Chem. Soc.* **2007**, *129*, 14 870–14 871.

[12] N. Bala Saidulu, K. L. Sebastian, *J. Chem. Phys.* **2008**, *128*, 074 708.

[13] A. Najafi, R. Golestanian, *Phys. Rev. E* **2004**, *69*, 062 901.

[14] D. J. Earl, C. M. Pooley, J. F. Ryder, I. Bredberg, J. M. Yeomans, *J. Chem. Phys.* **2007**, *126*, 064 703.

[15] D. C. Rapaport, *Phys. Rev. Lett.* **2007**, *99*, 238 101.

[16] G. Rückner, R. Kapral, *Phys. Rev. Lett.* **2007**, *98*, 150 603.

[17] Y.-G. Tao, R. Kapral, *J. Chem. Phys.* **2008**, *128*, 164 518.

[18] The internuclear separation between the catalytic head and the first polymer bead is fixed at a distance of r_{CN} by a holonomic constraint, which prevents the discontinues potential changes when chemical reaction occurs on the catalytic sphere.

[19] K. Tucci, R. Kapral, *J. Chem. Phys.* **2004**, *120*, 8262–8270.

[20] K. Kremer, G. Grest, *J. Chem. Phys.* **1990**, *92*, 5057–5086.

[21] J. M. Yeomans, *Physica A* **2006**, *369*, 159–194.

[22] R. D. Groot, P. B. Warren, *J. Chem. Phys.* **1997**, *107*, 4423–4435.

[23] A. Malevanets, R. Kapral, *J. Chem. Phys.* **1999**, *110*, 8605–8613.

[24] A. Malevanets, R. Kapral, *J. Chem. Phys.* **2000**, *112*, 7260–7269.

[25] R. Kapral, *Adv. Chem. Phys.* **2008**, *140*, 89–146.

[26] G. Gompper, T. Ihle, D. M. Kroll, R. G. Winkler, *Adv. Polym. Sci.* **2009**, *221*, 1–87.

[27] Dimensionless LJ units are used to report energy ε, mass m and distance σ parameters in the simulations: $r/\sigma \to r$, $t\sqrt{(\varepsilon/m\sigma^2)} \to t$ and $k_BT/\varepsilon \to T$. Energy parameters are chosen to be $\varepsilon = \varepsilon_C = \varepsilon_A = 1.0$ and $\varepsilon_B = 0.1$. Other parameters are $\alpha = 90^\circ$ (rotation angle), $\Delta t = 0.01$ (MD time step), $\tau = 0.5$ (MPC time), and $T = 1/3$ (temperature). The volume V consists of 40^3 MPC cells with unit volume. The total number of solvent particles is 640 000 so that the average number density is ≈ 10 molecules per unit volume. The masses of both A and B species are $m = 1$, while the masses of the catalytic C sphere and polymer beads are adjusted according to their diameters to ensure that the polymer chain is approximately neutrally buoyant.

[28] J. Happel, H. Brenner, *Low Reynolds Number Hydrodynamics*, Nijhoff, Dordrecht, **1965**.

Received: December 10, 2008